

THE IMPLEMENTATION OF IMAGE CLASSIFICATION AND ANALYSIS OF MRSD USING THREE DIFFERENT CLASSIFIERS: A CASE STUDY OF NEWCASTLE - UK

Huda M. Salih¹, Nada M. Salih²

^{1,2} University of Diyala, College of Engineering Iraq-Diyala
E-mail: huda_alansari@rocketmail.com, nada.flower@gmail.com

ABSTRACT: - Remote sensing data is an important data source that can provide valuable information about urban expansion and urban land cover and land use changes at various scales. Due to the increasing spatiotemporal dimensions of the remote sensing data, traditional classification algorithms may not be able to classify such data. In this regards, two key issues should be taken into account: firstly, the challenges of the images fusion of the optical multi-source remote sensing data (MRSD) to seek the possibility of improvement in classification accuracy for urban change mapping. Secondly, monitoring and detecting the change and the interrelationship between land cover and land use within urban areas are spectrally and spatially complex.

Therefore, this paper aims to test and compare three classification algorithms (maximum likelihood (ML), decision trees (DT), and support vector machines (SVM)) for their ability to infer and extract urban land cover/land use across five different years using Landsat 5 TM, Landsat 7 ETM+ and ASTER images. Image pre-processing and post-processing were conducted on each scene along five different dates to obtain classification maps of Newcastle city, UK. Thereafter, the three aforementioned classifiers were used and applied on the combined data, which contained thirty-three bands in order to evaluate their effectiveness at separating urban land cover/land use types.

The classification approaches were implemented using ERDAS IMAGINE 2013 and coding by MATLAB. The results indicate that the overall accuracy of three classification maps using ML, DT, and SVM classifiers was 71.09%, 73.05% and 83.20%, respectively. The classification maps present significant enhancement in the spectral and spatial resolution using optical MRSD compared to the one source of remote sensing data.

Keywords: Data fusion, Machine learning, Image classification, Multi-source remote sensing data, Urban Land cover/Land use, Support Vector Machine (SVM).

1. INTRODUCTION

Remote sensing images are widely used for monitoring urban expansion and mapping urban land cover/land use at a range of spatial and temporal scales, to improve the observation and understanding of change in the urban environment (Peijun *et al.*, 2012). Land cover and land use are a key driver of urban change, and have important implications for environmental issues (Jiao *et al.*, 2012). In order to extract urban land cover/land use maps, the accuracy and value of the derived land cover/land use maps are dependent on a range of factors related to the datasets and methods used (Foody, 1996). Further, the heterogeneity in urban landscapes often results in spectral and spatial variation within the land cover types (Bhatta, 2010). In order to recognise the complexity of the urban area, it is important at the beginning to test the ability of the remote sensing dataset and the methods of distinguishing

spectral signatures from the inherently mixed pixels in the urban environment(Lu and Weng, 2006).

Regarding the dataset, thirty three bands from Landsat and ASTER images were used in this work as optical multi-source remote sensing data (optical MRSD). The reason for using this number of bands on different dates is to evaluate their effectiveness at separating urban land cover/land use types, and this feature (multi-spectral image in different dates) will be exploited later in detecting urban change. This is because these images are temporal images(Schneider, 2012).Another reason for using this number of bands is to test the ability of the methods which will be used to handle and deal with the large dimensions of the remote sensing data(Hubert-Moy *et al.*, 2001). In addition, it is necessary to estimate their ability to improve classification accuracy on deriving land cover and land use classes.

Remote sensing image classification is one of the most significant applications for remote sensing (Perumal and Bhaskaran, 2010). A number of image classification algorithms have proven to have good precision for classifying remote sensing data(Mantero *et al.*, 2005). Therefore, of late, due to the increasing spatiotemporal dimensions of the remote sensing data, traditional classification algorithms may not be able to classify such data.Perumal and Bhaskaran (2010)argued that the traditional classification approaches have exposed weaknesses necessitating further research in the field of remote sensing image classification. Thus, an efficient classifier is needed to classify the remote sensing images to extract information(Foody and Mathur, 2004). To this end, machine learning approaches were adopted and compared with the conventional supervised classification approaches. The experimental work focused on image classification and analysis of urban area. This paper includes extracting the urban land cover/land use classification maps. The main objective of this paper is to test and compare three classification algorithms (maximum likelihood (ML), decision trees (DT), and support vector machines (SVM)) for their ability to infer and extract urban land cover/land use across five different years in one study area/city (from the selected cities). The second objective is to compare the accuracy of classes and the overall accuracy of classification of this selected city. The third objective is to evaluate and deduce the use of optical MRSD in separating urban land cover/land use classes rather than one remote sensing data source.

2. DATA ACQUISITION

2.1 Remote sensing data

Landsat Thematic Mapper (TM) images and Enhanced Thematic Mapper Plus (ETM+) for the city of Newcastle were obtained from the Aeronautics and Space Administration/ the U.S. Geological Survey (USGS GLOVIS), United States of America. The website for free Landsat image download was: <http://glovis.usgs.gov>. The Advanced Space-borne Thermal Emission and Reflection Radiometer (ASTER) scene and the advanced space.

Landsat 5 TM, Landsat 7 ETM+ and ASTER images were used in this work as different optical sources, as they were available on different dates: 1992, 2000, 2002, 2003 and 2011. These images include VNIR and SWIR bands, which are six bands in each scene of Landsat data and nine bands of ASTER data with a spatial resolution of 30m and 15m, respectively. We choose Newcastle city because the data of this city was available.

It was decided to employ these medium spatial resolution images for four reasons: (1) they are available to achieve the purpose of this work; (2) increasing spectral variability within-class can reduce class separability and classification accuracy when using high spatial resolution images(Van de Voorde *et al.*, 2011); (3)there is improved and increased spatial resolution of Landsat images through using the VNIR bands of ASTER images (4) there were increased numbers of spectral bands, even with the same spectral characteristics of Landsat images, because the aim for this study is to evaluate the performance of the selected classifiers in dealing with such a large dataset for classifying and fusing MRSD (later) and implement the whole research.

2.2 The study area location

A part of the city of Newcastle was selected as a study area to achieve this experimental work. This city and its metropolitan borough are located in Tyne and Wear, North East England. Its geographical coordinates are:

54° 58' 26.4" N, 1° 36' 47.52" W, (Google earth), as shown in figure (1).

3. METHODOLOGY

3.1 Remote Sensing Data Pre-Processing and Correction

Radiometric and geometric corrections, and the accurate registration of the different years of the remote sensing images, are the key factors in monitoring urban changes (Vogelmann *et al.*, 2001). The geometric corrections were done with the L1B data product of Landsat and ASTER scenes. The ASTER scene was co-registered to the Landsat scene, which had been acquired in UTM projection. Nearest neighbour re-sampling was applied when assigning pixel value for all scenes. Radiometric correction was necessary to reduce and eliminate differences due to a sensor variation. Thus, the raw digital number (DN) values of Landsat and ASTER images were converted to reflectance values. Atmospheric correction, however, was not achieved because the purpose of this work was just to evaluate image classification and analysis outcomes without extracting any changes in the city.

3.2 Image sub-setting and stacking

All the image files were reduced to cover only the area of interest (AOI). This AOI represents a part of the city of Newcastle of around 197.32km². A combined/stacked image was created by stacking all the bands of these images (four images of Landsat and one image of ASTER) using ERDAS IMAGINE 2013. This process can speed up processing (image classification) because all the subset bands of images can be classified together and, in addition, can be used to improve classification accuracy (Bhatta, 2012). Therefore, this combined/stacked image includes thirty three bands of five images (6 bands in each 4 images of Landsat and 9 bands of ASTER image). The spatial resolution of this image was automatically resampled to become 18.23m during the process of stacking. This means that the spatial resolution of four images of Landsat was enhanced and improved by the spatial resolution of ASTER image. Figure (2) shows the stacked image on different dates, ready to classify and derive urban land cover/land use.

The large number of bands in this image allowed for a wide range to perceive the change between these bands in order to obtain the best visually spectral band combination (viewing of the three bands combination using ERDAS IMAGINE). The next step of this methodology was to conduct the classification, and thus the combination of spectral bands and their correlations were tested and checked when collecting training areas to extract the classified maps. For example, man-made materials such as concrete and asphalt both display spectral curves that generally increase from the visible through the Near IR and Mid-IR regions. The spectral band combination, therefore, was bands 1, 4 and 7. However, as concrete ages, it becomes darker and as asphalt ages it becomes lighter; this can be observed with these urban surface materials through different dates of the combined images used in this work.

3.3 Image Classification

Classification of land cover and land use is an important and difficult task, since such images are highly dimensional and complex in nature. Remote sensing images can be classified as supervised and unsupervised. In this work, the supervised image classification was adopted because it is much more accurate for mapping information classes. However, this approach depends on the cognition and skills of the image analyst. The user's experience can be very helpful in identifying and locating training areas (Tso and Mather, 2009). The combined image produced from Landsat and ASTER datasets was independently classified using three approaches: Maximum Likelihood, Decision Tree and Support Vector Machine. Each of these algorithms is based on a different mathematical theory that is described with a method of applying them in the following sections. Information obtained from aerial photographs helped in identifying sample pixels for land cover/land use category on the

imagery. The classifiers use the properties of such sample pixels, known as training pixels, to work out parameters for the land cover classes to which each pixel on the imagery would be assigned. The classification process generates thematic maps on which different land cover and land use categories are generally presented in different colours.

The land cover and land use classes were chosen to achieve the aims of this work are water, bare soil, trees, grass, roads, built-up areas (residential areas) and built-up areas (commercial and industrial areas). The reason for using different colours between these generated maps is to clearly recognise the boundaries between the generated classes in each map, because it is difficult to distinguish these boundaries visually with the same colours, especially those between residential and commercial/industrial areas in the built-up class. This is due to a small dispersed area of commercial/industrial area compared to residential areas in the built-up class in the study area. However, the comparison between the produced classification maps, perhaps, is difficult due to using a different colour labelling scheme, but the actual comparison in this work was done depending on the statistical computations for each class. Consequently, the comparison of urban land cover/land use was more reliable in terms of the estimation of the accuracy in assigning these classes. Furthermore, it was decided to extract and classify land cover and land use classes together in each thematic map produced from these classifiers. This is because the purpose of this work is to test and evaluate the ability of these classifiers to separate between land cover and land uses classes in the urban area using two optical sources of remote sensing datasets. Then, by recognising and identifying this ability of each classifier in this work, it is expected that there will be the ability to classify urban land cover and land use on separate maps.

3.3.1 Image Classification using Maximum Likelihood (ML) Classifier

The Maximum Likelihood (ML) classifier is one statistical classifier that relies on the normal distribution of the data in each class. The geometrical shape of a number of pixels belonging to a class is represented by an ellipsoid. The locations, shapes and sizes of the ellipsoids are derived from the means and variance-covariance matrices of the classes.

These ellipses represent the contours of conditional probability of membership, the values of which decline with distance from the mean centre. Distance from the centre is not the only criterion for deciding whether a pixel belongs to one class or another. The shape of the conditional probability contours depends on the relative dimensions of the axes of the ellipse as well as on its orientation. The resulting classification might be expected to be more accurate than other statistical ones because the training sample data are being used to provide estimates of the shapes of the distribution of membership of each class in the n-dimensional feature space, as well as of the location of the centre point of each class (Murthy *et al.*, 2003)

It is important to take into consideration that a ML classifier gives good results if the frequency distribution of the data is in the multivariate normal distribution. Unsupervised classification methods can be used to find out whether training data represents the assumption of normal distribution. After estimating the conditional probabilities of each pixel being a member of a class, the most likely class having the highest probability value is assigned to the pixel with a class label. If the highest probability value of a pixel is lower than a threshold to be set by an analyst, then the pixel is labelled as unclassified. Based on the Bayes theorem, which states that the a posteriori distribution $P(i|\omega)$, i.e., the probability that a pixel with feature vector ω belongs to class i , is given by:

$$P(i|\omega) = \frac{P(\omega|i)P(i)}{P(\omega)} \quad (1)$$

Where $P(\omega|i)$ is the likelihood function, $P(i)$ is the a priori information, i.e., the probability that class i occurs in the study area and $P(\omega)$ is the probability that ω is observed, which can be written as:

$$P(\omega) = \sum_{i=1}^M P(\omega | i)P(i) \quad (2)$$

Where M is the number of classes. $P(\omega)$ is often treated as a normalization constant to ensure $\sum_{i=1}^M P(i | \omega)$ sums to 1. Pixel x is assigned to class i by the rule:

$$x \in i \quad \text{if } P(i|\omega) > P(j|\omega) \quad \text{for all } j \neq i \quad (3)$$

ML often assumes that the distribution of the data within a given class i obeys a multivariate Gaussian distribution. It is then convenient to define the log likelihood (or discriminant function):

$$g_i(\omega) = \ln P(\omega | i) = -\frac{1}{2}(\omega - \mu_i)^t C_i^{-1}(\omega - \mu_i) - \frac{N}{2} \ln(2\pi) - \frac{1}{2} \ln(|C_i|) \quad (4)$$

Since log is a monotonic function, Equation (3) is equivalent to:

$$x \in i \quad \text{if } g_i(\omega) > g_j(\omega) \quad \text{for all } j \neq i. \quad (5)$$

Each pixel is assigned to the class with the highest likelihood or labeled as unclassified if the probability values are all below a threshold set (Asmala Ahmad, 2012).

To implement ML classification, it requires the selection of training samples by defining a polygon in the image representing a class of land cover and land use through using AOI tools. Then, the data file values in the training sample are used to create a signature. The signature is then used in the classification process, because a classification decision rule (algorithm) requires some signature attributes as input.

On this basis, the combined/stacked image was classified and the land cover/land use classes were selected and recognised for training areas. The classes were bare soil, trees, grass, built-up areas (residential areas) and built-up areas (commercial and industrial areas), as shown in figure (3). These classes were selected and derived from the original image because they represent the most common surfaces found in urban material in which change can occur. Therefore, it was important to extract these classes of the urban land cover/land use classes and recognise them using the classification process. ML classification was implemented by ERDAS.

3.3.2 Image Classification using a Decision Tree (DT) Classifier

The second classifier used was a decision tree (DT). This classifier has been used increasingly in remote sensing studies in recent years. A classification approach based on DT does not require assumptions regarding the distribution of the data and it can be used to create classification rules automatically from a large number of input attributes (Pal and Mather, 2003). DT classification have been used for urban/suburban land cover/land use classification studies because a hierarchical structure for labelling objects can help to gain a more comprehensive understanding of relationships between urban objects at different scales of observation or at different levels of detail (Li *et al.*, 2012).

A hierarchical decision tree classifier is an algorithm for the labelling of an unknown pattern using a sequence of decisions. A decision tree is composed of a root node, a set of interior nodes, and terminal nodes called leaf nodes. The root node and interior nodes, referred to collectively as non-terminal nodes, are linked into the decision stages. The terminal nodes represent the final classification. The classification process is implemented by a set of rules that determine the path to be followed, starting from the root node and ending at one terminal node, which represents the label for the object being classified. At each node, a decision has to be made about the path to the next node. The nature of the decisions being set and the sequence of attributes occurring within a tree will affect classification results. Thus,

one knows that the efficiency and performance of this approach is strongly affected by the algorithm for inducing a decision tree.

The class distribution of the records $\mathbf{p}(i|t)$ of the fraction of records $\mathbf{p}(i|t)$ before and after splitting belonging to class i at a given node t . The based split of classes can be obtained, as follows:

$$\text{Entropy}(t) = - \sum_{i=0}^{c-1} p(i|t) \log_2 p(i|t), \quad (6)$$

$$\text{Gini}(t) = 1 - \sum_{i=0}^{c-1} [p(i|t)]^2, \quad (7)$$

$$\text{Classification error}(t) = 1 - \max_i [p(i|t)], \quad (8)$$

Where c is the number of classes and $0 \log_2 0 = 0$ in the entropy calculation (Zaiiane, O.R. 1999).

In this work, the design of a decision tree to classify the same study area was implemented by a graph of the spectral range in each band and statistics for all classes. The observations of the spectral values of each band were done manually in order to gain an idea of the highest spectral values (or the values which can be distinguished from others) for deriving urban classes. Afterwards, the statistical computations (rules) were used to estimate the decision boundaries of classes automatically, and the tree is designed to separate classes in a hierarchical fashion, as shown in appendix (A). The same urban land cover/land use classes were derived in addition to the possibility of deriving the roads. This classification approach was implemented using ERDAS, and the outcome is represented in figure (4).

To generate each class into the decision tree, for example, the class one, which represents water, has a very high spectral value in band (10) and band (16) (which is NIR band of the combined image-(33) spectral bands). These values were 0.0946 and 0.1127, respectively. Thus, class one can be extracted from other classes through creating the following rule: IF Band10 \leq 0.0946 OR Band16 \leq 0.1127 \rightarrow Water, ELSE (another class will be extracted depending on the bands values), as shown in appendix (A). Similarly, each band was examined as a variable in order to set the rule or requirement for deriving each category. In the end, a set of conditions and rules were gathered that were used to derive the rest of categories.

3.3.3 Image Classification using a Support Vector Machine (SVM) Classifier

A support vector machine (SVM) represents a group of theoretically superior machine learning algorithms. The principle of SVM classification can be described as follows. Through mapping the input vectors into the high-dimension space, SVM searches for the optimal hyperplane to separate the training vectors of two classes into two sub-spaces. Such a separation hyperplane is subject to the condition that the margin of separation between the first and second class samples is maximized. Therefore, the class of the test vector will be decided according to which sub-space it will be mapped in. Therefore, SVM is originally a binary classifier (Mountrakis *et al.*, 2011). With the SVM classification, it is not necessary for all the training samples to contribute to the building of the hyperplane, but normally only a subset of training samples is chosen as support vectors and this attribute is unique to SVMs.

The data for training is a set of points (vectors) x_i along with their categories y_i . For some dimension d , the $x_i \in \mathbb{R}^d$, and the $y_i = \pm 1$. The equation of a hyperplane is

$$\langle \mathbf{w}, \mathbf{x} \rangle + \mathbf{b} = 0, \quad (9)$$

where $\mathbf{w} \in \mathbb{R}^d$, $\langle \mathbf{w}, \mathbf{x} \rangle$ is the inner (dot) product of \mathbf{w} and \mathbf{x} , and \mathbf{b} is real.

The following problem defines the best separating hyperplane. Find \mathbf{w} and \mathbf{b} that minimize

$\|w\|$ such that for all data points (x_i, y_i) ,

$$y_i(\langle w, x_i \rangle + b) \geq 1. \quad (10)$$

The support vectors are the x_i on the boundary, those for which $y_i(\langle w, x_i \rangle + b) = 1$.

For mathematical convenience, the problem is usually given as the equivalent problem of minimizing $\langle w, w \rangle / 2$. This is a quadratic programming problem. The optimal solution (\hat{w}, \hat{b}) enables classification of a vector z as follows: (Hastie, T., R., 2008).

$$\text{class}(z) = \text{sign}(\langle \hat{w}, z \rangle + \hat{b}). \quad (11)$$

This classification approach was implemented using Matlab codes because there is no tool in the existing software to perform this classification. This is because SVM is considered one of the new methods of the learning machine. In this work, as with any supervised learning model, the training point sets for each class were collected first, as in appendix (B), and then an SVM was trained. Third, the trained machine was used to classify (predict) new data (the rest pixels). This is done through creating a program using Matlab codes, as in appendix (B). The mathematical approach of SVM using kernels relies on the computational method of hyperplanes. All the calculations for hyperplane classification use nothing more than dot products. For this, in this program, a window for displaying each band of the combined image was created in order to collect the dots, which represent the training point sets of each class, and then stored as a matrix of data points. The *svmtrain* function was used for this purpose. The validation of training point sets was also coded. Afterwards, new data were classified using the *svmclassify* function. The creation, labelling and display of the outputs as a final classification map were scripted in Matlab. In order to evaluate the performance of the SVM classifier, two classification maps were produced. One map includes the same urban land cover/land use classes as aforementioned in the ML classification; another map includes the class of road in addition to these classes as aforementioned in DT classification. These maps are shown in figures (5) and (6).

3.4 Accuracy assessment

In order to determine the accuracy of the classification, it is necessary to determine if the output map meets, exceeds, or does not meet certain predetermined classification accuracy criteria. A most common and typical method used by researchers to assess classification accuracy is with the use of an error matrix (sometimes called a confusion matrix or contingency table) (Congalton and Green, 2008). This table compares known reference data to the corresponding classification results (Myeong *et al.*, 2001). In this work, accuracy assessment was conducted on all the classification maps by creating 256 reference pixels randomly, using ERDAS IMAGINE, in order to provide information on the accuracy of each of the classifications. Congalton and Green (2008) state that it has been shown that more than 250 reference pixels are needed to estimate the mean accuracy of a class to within plus or minus five percent. Thus, this number of reference pixels, used for such a small area of the study area, was sufficient to assess the accuracy of classification. After conducting the registration between the reference information and classified maps, aerial photos of the city of Newcastle with a recent date (2013), with a high spatial resolution of 10 cm, were used as the existing source of reference information in order to assess classification accuracy by comparison of them. The results are presented in tables (1), (2) and (3) for three classification maps.

4. THE RESULT

The outcomes from examining three different classification approaches using ML, DT, and SVM classifiers are presented in this section. The outcomes include thematic maps (the classification maps) of the urban land cover and land use classes as well as the confusion matrices. The overall accuracy of three classification maps was 71.09%, 73.05% and 83.20%, respectively. The outcomes revealed the possibility of distinguishing built-up classes (residential and commercial/industrial areas) from other land cover classes through using optical MRSD. However, the results showed a discrepancy between the ability of classifiers

in the extraction urban land cover and land use classes, as follows in fig (3 to 6) &table (1 to 3).

5. DISCUSSION OF RESULTS

In spite of the numerous challenges inherent in moderate-spatial resolution images, the methods were able to produce a general cover classification for the city of Newcastle. There are three main results from this work. First, the cross-validation accuracies from the final maps show the non-parametric supervised classification (DT and SVM) was better than the parametric supervised classification (ML). Overall accuracy was 73.05%, 83.20% and 71.09%, respectively. Especially, the performance of SVM outperformed on both of DT and ML classifiers. Although the SVM classifier outperformed the DT and ML classifiers in inferring and deriving urban land cover and land use classes, all pixels of the stacked image were classified by all these classifiers and there were no unclassified pixels.

Second, in the final classification maps, which were derived from DT and SVM, the class of road was possible to recognise from the six other classes; however, the accuracy of the ML classification outcomes was unsatisfactory when attempting to derive this class. At the same time, the overall accuracy of the SVM classification increased in figure (6) compared to the map in figure (5), at 83.20% and 81.75%, respectively. However, the classification map of a combined/stacked image by the ML classifier was better than the classification map derived from one date of the Landsat image because this map shows a great deal of overlapping between urban land cover/land use classes, especially between built-up classes, as shown in figure (7). In this figure, it was decided to compare the classification map derived from one remote sensing source (e.g. Landsat 5 TM, six bands, in 2011) and another derived from a combined image, which is used in this work (four images from Landsat and one image from ASTER). The purpose of this was to evaluate increased spectral and spatial resolution through stacking other bands from different dates of Landsat and employing another source with higher spatial resolution, such as ASTER. The figure shows that the map on (b) was better than the map in (a) in terms of separating surface materials in urban areas, especially for residential areas from commercial/industrial areas. However, there was a clear overlap between two classes of built-up areas using one source of remote sensing. The map was classified by ML with the same labelling and colour scheme in order to present this variance.

Third, although the land cover and land use classes of the urban were a distinct area across the classifiers, a significant difference appeared between these classes. A number of specific difficulties arose as shown by the relatively low individual accuracies for a few classes. The classification using the original thirty three bands of moderated-spatial resolution imagery revealed difficulty in identifying the seven classes by DT and SVM, and six classes by ML, because some of the features have similar spectral responses with other classes. For example, in ML classification, the omission error of bare soil was 95%, which means there was overlap in the spectral response between this class and other classes. The commission error of built-up class (residential area) was 15.49% overlapping between this class and (bare soil, built-up-commercial/industrial and road) class. Specifically, confusion occurred between bare soil and impervious surfaces, grass and trees over all classification approaches. These spectral similarities are especially evident when using only the two optical sources of remote sensing data, in spite of the improvements in the classes' separation. Therefore, there is a trade-off between the need for spatial detail and increased specificity of cover classes.

The bare soil class had low classification accuracy. However, the commission and omission errors of bare soil were relatively large. This is because the collected soil samples from image were not stratification of the actual ground truth due to the overlapping with other classes. The misclassification of soil occurred mostly with grass or impervious surfaces. It is likely that the confusion between grass and bare soil is because bare soil often exists within or near the grass cover type (e.g. thin grass cover or pathways). Thus, the edge pixels

located between grass and bare soil may cause low accuracy for bare soil. Further, the reference pixels for grass and bare soil contained varying levels of vegetation density leading to an indistinct assignment of the discrete classes. The confusion of bare soil with impervious surfaces is likely because urban bare soil usually has a spectral response that is similar to the man-made surfaces. Nevertheless, table (3) presents a higher accuracy of separation of the bare soil with other classes compared to ML and DT in tables (1) and (2) at 76.19%, 4.76% and 64.10%, as the producer's accuracy, respectively. Similarly, the average of the producer's accuracies for both of built-up areas (residential and commercial/industrial areas) was 81.73% in the SVM classification, 69.09% in the DT classification and 47.80 % in the ML classification.

6. CONCLUSION

Three different classification approaches were implemented and their results evaluated. MRSD, which includes the three optical sources data: Landsat 5 TM, Landsat 7 +ETM and ASTER, was also evaluated in terms of the improvements of urban land cover/land use of the city of Newcastle. The classification maps show significant enhancement in the spectral and spatial resolution using optical MRSD compared to the one source of remote sensing data. Hence, enhanced urban land cover/land use classification occurred. However, there is still concern about the apparent confusion between urban land cover/land use classes in terms of the spectral similarity between the surfaces of these classes. Therefore, the inclusion of a texture measure, perhaps, reduces this confusion. Myeong *et al.* (2001) stated that additional information, such as texture information, can improve classification between grass/herbaceous and trees/shrubs, and between bare soil and impervious surfaces. That means the additional remote sensing data source (using a different range of spectrum wavelengths, such as thermal bands and/or radar) can be beneficial to separate between such classes.

Regarding the performance of the tested classifiers, the non-parametric supervised classifier (machine learning algorithm for image classification), such as the DT and SVM classifiers outperformed the parametric supervised classifier (the conventional statistical methods), such as the ML classifier. This is because these methods usually do not require any prior assumptions about the distribution of input data, as is the case for the maximum likelihood classifier, since they are usually better suited for the classification of multisource data sets (Waske and Benediktsson, 2013). Therefore, it was decided to implement this experimental work as a part of the whole of paper in order to consider the advantages and limitations of the use of MRSD in separating urban land cover/land use before commencing with the actual implementation of the research work.

REFERENCES

- 1) Asmala Ahmad. (2012) *Analysis of Maximum Likelihood Classification on Multispectral Data*, Hang Tuah Jaya, 76100 Durian Tunggal, Melaka, Malaysia
- 2) Bhatta, B. (2010) *Analysis of Urban Growth and Sprawl from Remote Sensing Data*. Berlin: Springer.
- 3) Bhatta, B. (2012) *Urban Growth Analysis and Remote Sensing A case study of Kolkata, India 1980-2010*. London: Springer.
- 4) Congalton, R.G. and Green, K. (2008) *Assessing the accuracy of remotely sensed data: principles and practices*. CRC press.
- 5) Foody, G.M. (1996) 'Relating the land-cover composition of mixed pixels to artificial neural network classification output', *Photogrammetric Engineering and Remote Sensing*, 62(5), pp. 491-498.
- 6) Foody, G.M. and Mathur, A. (2004) 'Toward intelligent training of supervised image classifications: directing training data acquisition for SVM classification', *Remote*

- Sensing of Environment*, 93(1–2), pp. 107-117.
- 7) Hastie, T., Tibshirani, R. and Friedman, J. (2008) *The Elements of Statistical Learning*, second edition. Springer, New York.
 - 8) Hubert-Moy, L., Cotonnec, A., Le Du, L., Chardin, A. and Perez, P. (2001) 'A comparison of parametric classification procedures of remotely sensed data applied on different landscape units', *Remote Sensing of Environment*, 75(2), pp. 174-187.
 - 9) Jiao, L., Liu, Y. and Li, H. (2012) 'Characterizing land-use classes in remote sensing imagery by shape metrics', *ISPRS Journal of Photogrammetry and Remote Sensing*, 72(0), pp. 46-55.
 - 10) Li, A., Jiang, J., Bian, J. and Deng, W. (2012) 'Combining the matter element model with the associated function of probability transformation for multi-source remote sensing data classification in mountainous regions', *ISPRS Journal of Photogrammetry and Remote Sensing*, 67(0), pp. 80-92.
 - 11) Lu, D. and Weng, Q. (2006) 'Use of impervious surface in urban land-use classification', *Remote Sensing of Environment*, 102(1), pp. 146-160.
 - 12) Mantero, P., Moser, G. and Serpico, S.B. (2005) 'Partially supervised classification of remote sensing images through SVM-based probability density estimation', *Geoscience and Remote Sensing, IEEE Transactions on*, 43(3), pp. 559-570.
 - 13) Mountrakis, G., Im, J. and Ogole, C. (2011) 'Support vector machines in remote sensing: A review', *ISPRS Journal of Photogrammetry and Remote Sensing*, 66(3), pp. 247-259.
 - 14) Murthy, C.S., Raju, P.V. and Badrinath, K.V.S. (2003) 'Classification of wheat crop with multi-temporal images: performance of maximum likelihood and artificial neural networks', *International Journal of Remote Sensing*, 24(23), pp. 4871-4890.
 - 15) Myeong, S., Nowak, D.J., Hopkins, P.F. and Brock, R.H. (2001) 'Urban cover mapping using digital, high-spatial resolution aerial imagery', *Urban Ecosystems*, 5(4), pp. 243-256.
 - 16) Pal, M. and Mather, P.M. (2003) 'An assessment of the effectiveness of decision tree methods for land cover classification', *Remote Sensing of Environment*, 86(4), pp. 554-565.
 - 17) Peijun, D., Sicong, L., Gamba, P., Kun, T. and Junshi, X. (2012) 'Fusion of Difference Images for Change Detection Over Urban Areas', *Selected Topics in Applied Earth Observations and Remote Sensing, IEEE Journal of*, 5(4), pp. 1076-1086.
 - 18) Perumal, K. and Bhaskaran, R. (2010) 'Supervised classification performance of multispectral images', *arXiv preprint arXiv:1002.4046*.
 - 19) Schneider, A. (2012) 'Monitoring land cover change in urban and peri-urban areas using dense time stacks of Landsat satellite data and a data mining approach', *Remote Sensing of Environment*, 124(0), pp. 689-704.
 - 20) Tso, B. and Mather, P.M. (2009) *Classification methods for remote sensing data*. second edition edn. U.S.: Taylor & Francis Group.
 - 21) Vogelmann, J.E., Helder, D., Morfitt, R., Choate, M.J., Merchant, J.W. and Bulley, H. (2001) 'Effects of Landsat 5 Thematic Mapper and Landsat 7 Enhanced Thematic Mapper Plus radiometric and geometric calibrations and corrections on landscape characterization', *Remote Sensing of Environment*, 78(1), pp. 55-70.
 - 22) (Zaiiane, O.R. 1999). <http://www-users.cs.umn.edu/~kumar/dmbook/ch4.pdf>

Table (1): Error matrix for the stacked image (33 bands) classification of the city of Newcastle using a ML classifier.

Class name	Reference Data						Row total	User's accuracy (%)
	Water	Bare Soil	Trees	Grass	Built-up areas-residential areas	Built-up areas-commercial/Industrial areas		
Classified Data								
Water	4	0	0	0	0	0	4	100.00
Bare Soil	0	1	0	2	2	1	6	16.67
Trees	0	4	22	7	2	0	35	59.46
Grass	0	7	2	27	3	0	39	69.23
Built-up areas-residential areas	2	8	6	13	109	10	148	73.65
Built-up areas-com./ind. areas	0	1	0	0	4	19	24	79.17
Column total	6	21	30	49	120	30	182/256	
Producer's accuracy (%)	66.67	4.76	73.33	55.10	90.83	63.33	Overall accuracy 71.09% Overall Kappa 0.57	

Table (2): Error matrix for the stacked image (33 bands) classification of the city of Newcastle using a DT classifier.

Class name	Reference Data							Row total	User's accuracy (%)
	Water	Bare Soil	Trees	Grass	Built-up areas-residential areas	Built-up areas-commercial/Industrial areas	Road		
Classified Data									
Water	7	0	0	0	0	0	0	7	100.00
Bare Soil	0	25	4	7	10	0	3	49	51.02
Trees	0	2	13	2	1	0	1	19	68.42
Grass	0	1	0	22	0	0	0	23	95.65
Built-up areas-residential areas	0	3	0	0	60	4	4	71	84.51
Built-up areas-com./ind. areas	0	1	0	0	0	11	0	12	68.42
Road	0	7	1	7	10	1	49	75	65.33
Column total	7	39	18	38	81	16	57	187/256	
Producer's accuracy (%)	100.00	64.10	72.22	57.89	74.07	68.75	85.96	Overall accuracy 73.05% Overall Kappa 0.66	

Table (3): Error matrix for the stacked image (33 bands) classification of the city of Newcastle using a SVM classifier for figure (6).

Class name	Reference Data							Row total	User's accuracy (%)
	Water	Bare Soil	Trees	Grass	Built-up areas-residential areas	Built-up areas-commercial/Industrial areas	Road		
Water	18	0	0	0	0	0	0	18	100.00
Bare Soil	0	32	0	4	2	2	3	43	74.42
Trees	0	0	19	1	0	4	1	25	76.00
Grass	0	3	1	35	0	0	1	40	87.50
Built-up areas-residential areas	0	2	0	0	45	4	2	53	84.91
Built-up areas-com./ind. areas	0	3	0	0	2	40	1	46	86.96
Road	0	2	0	0	3	2	24	31	77.42
Column total	18	42	20	40	52	52	32	213/256	
Producer's accuracy (%)	100.00	76.19	95.00	87.50	86.54	76.92	75.00		Overall accuracy 83.20% Overall Kappa 0.66

*The overall accuracy of classification map by SVM in figure (5) was 81.75%

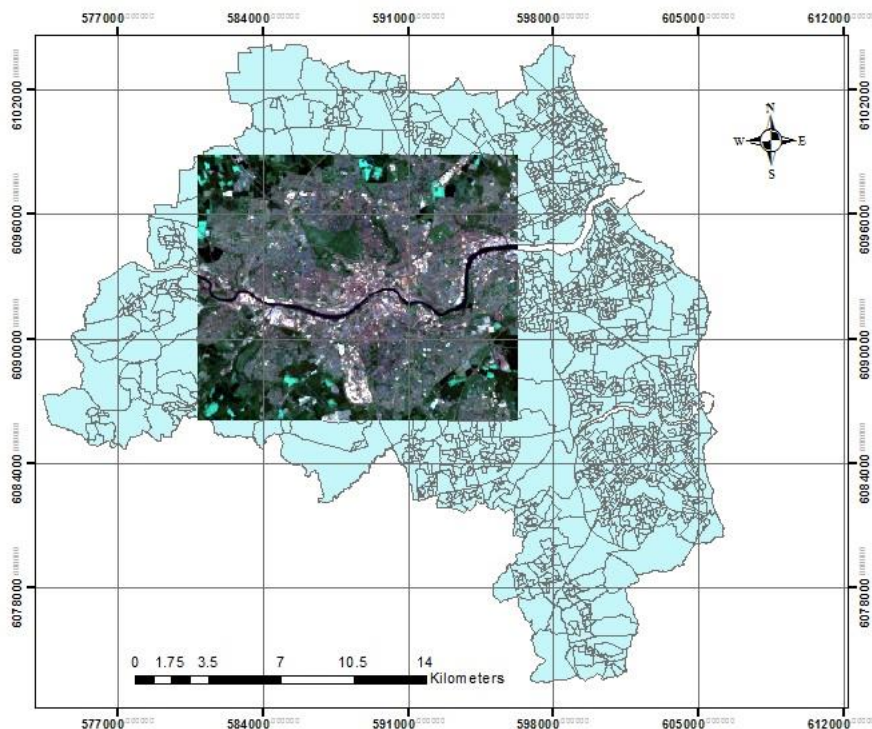


Figure (1): Map of the Study Area (Google earth).

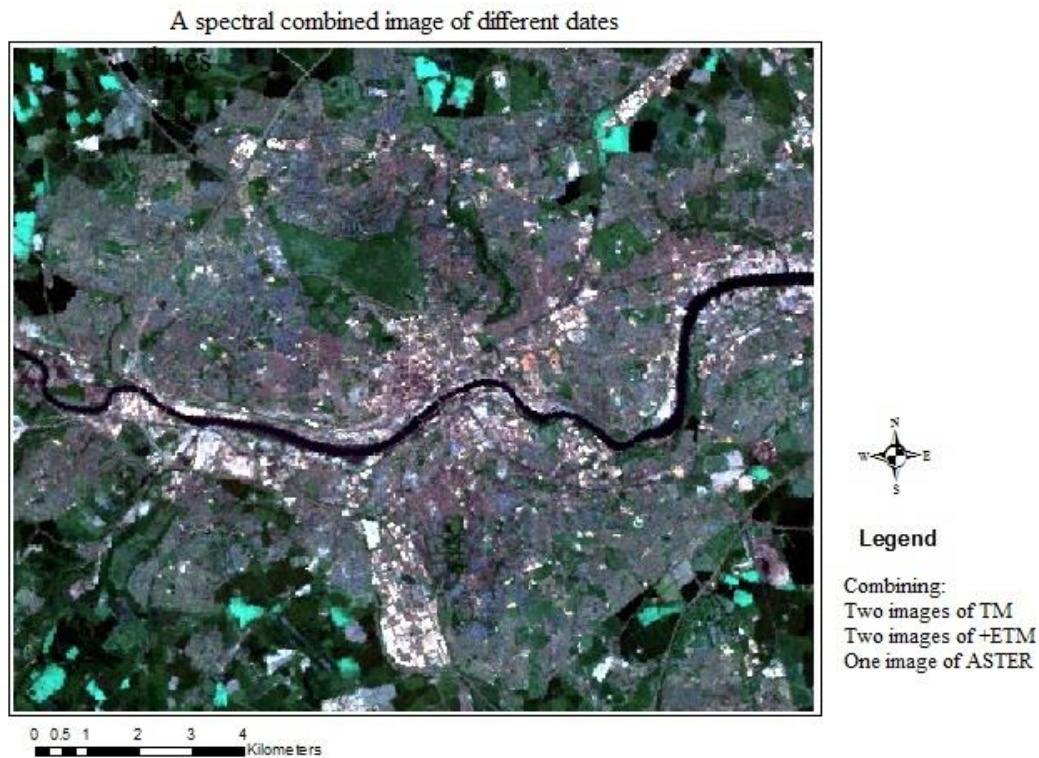


Figure (2): A combined image formed from the two Landsat 5 TM (in 1992 and 2011), two Landsat 7 +ETM (in 2000 and 2001) and ASTER images (in 2003).

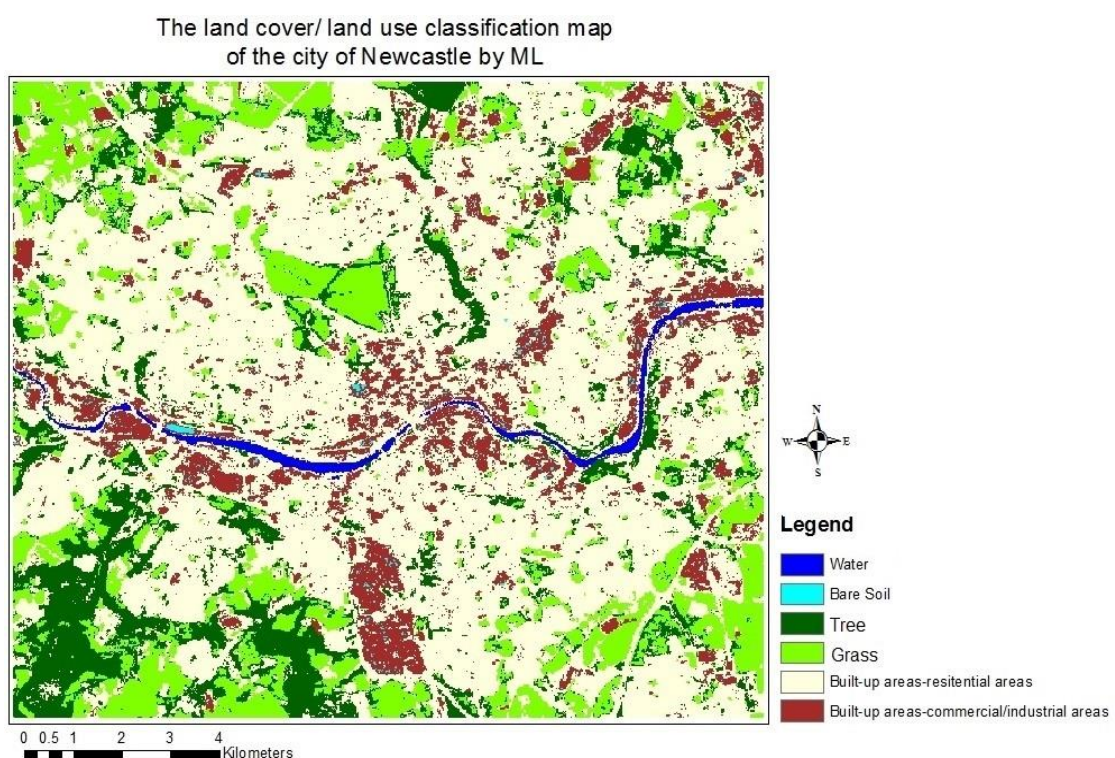


Figure (3): The city of Newcastle classification map using supervised ML classifier for the combined image of Landsat (in 1992, 2000, 2002 and 2011) and ASTER (in 2003)

The land cover/ land use classification map
of the city of Newcastle by DT

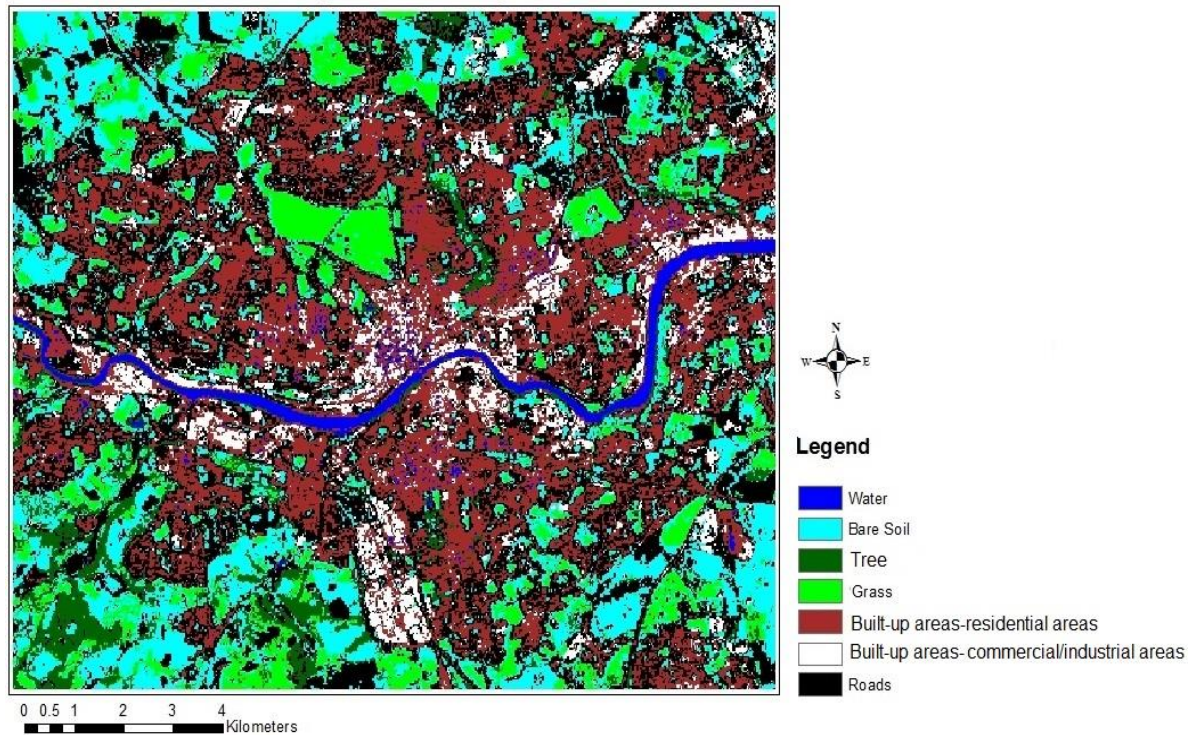


Figure (4): The city of Newcastle classification map using a supervised DT classifier for the combined image of Landsat (in 1992, 2000, 2002 and 2011) and ASTER (in 2003).

The land cover/ land use classification map
of the city of Newcastle by SVM

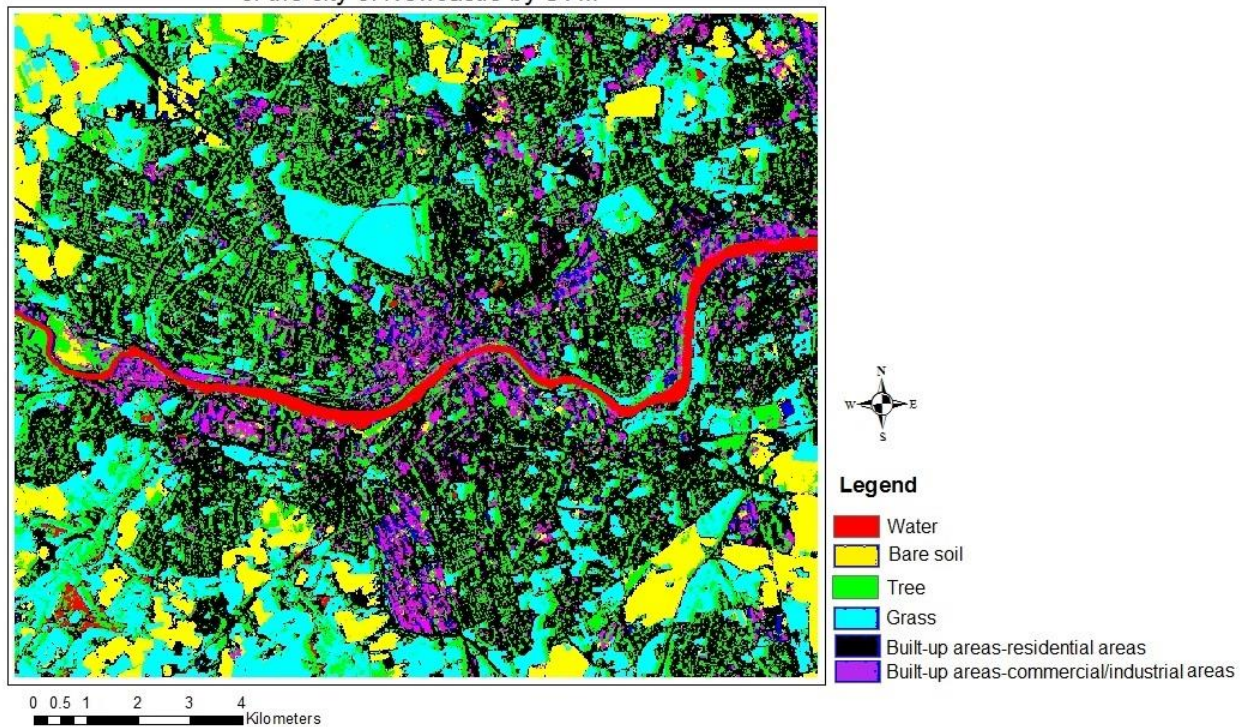


Figure (5): The city of Newcastle classification map using a supervised SVM classifier without the class of road classifier for the combined image of Landsat (in 1992, 2000, 2002 and 2011) and ASTER (in 2003).

The Land cover/ land use classification map
of the City of Newcastle by SVM

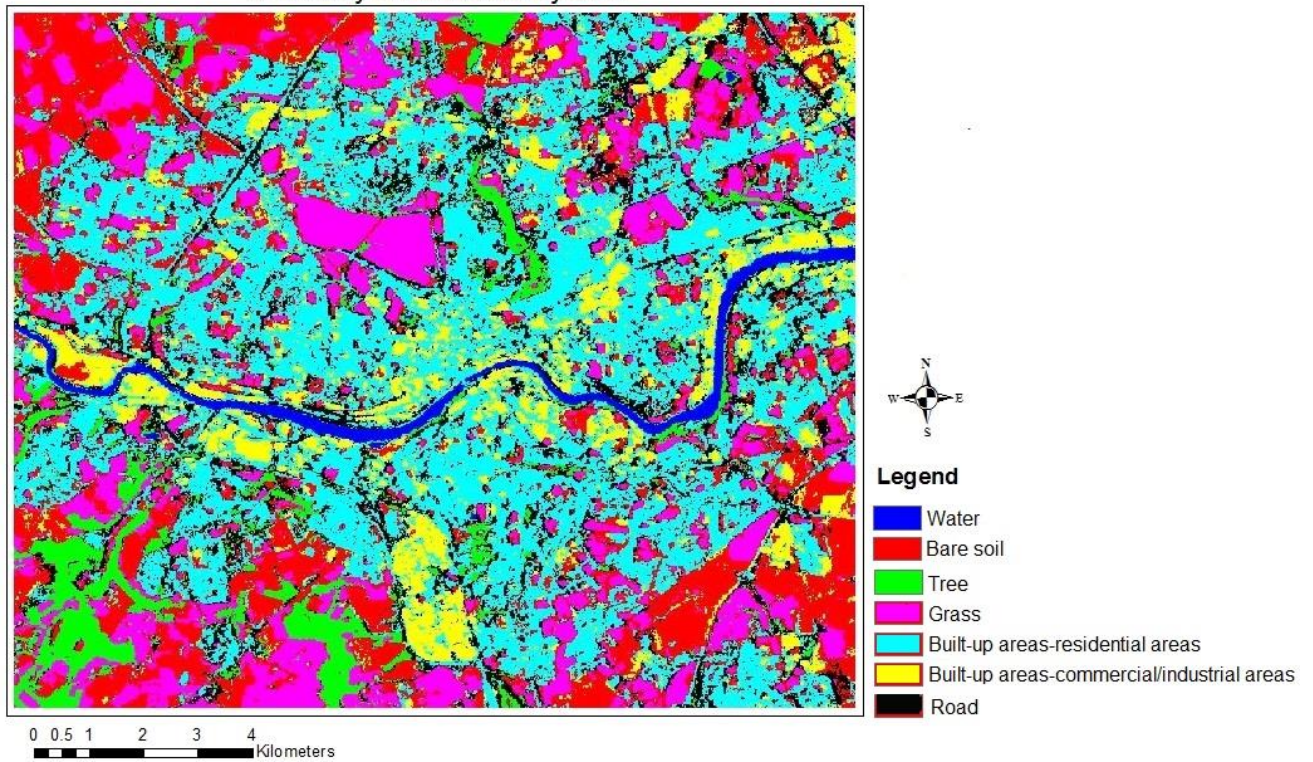


Figure (6): The city of Newcastle classification map using a supervised SVM classifier with the class of road classifier for the combined image of Landsat (in 1992, 2000, 2002 and 2011) and ASTER (in 2003).

تطبيق تصنيف الصور وتحليل بيانات الاستشعار عن بعد متعددة المصدر باستخدام ثلاث مصنفات مختلفة: دراسة حالة لمدينة نيوكاسل -المملكة المتحدة

ندى محمد صالح
كلية الهندسة / جامعة ديالى
Email: nada.flower@gmail.com

هدى محمد صالح
كلية الهندسة / جامعة ديالى
Email: huda_alansari@rocketmail.com

الخلاصة

بيانات الاستشعار عن بعد هي مصدر البيانات الهامة التي يمكن أن توفر معلومات قيمة حول التوسع العمراني والغطاء النباتي في المناطق الحضرية والتغيرات في استخدام الأراضي على مستويات مختلفة. نظرا للتنوع الكبير لبيانات الاستشعار عن بعد من حيث الدقة المكانية والزمانية ، قد لا تكون خوارزميات التصنيف التقليدية قادرة على تصنيف مثل هذه البيانات. وفقا لذلك ، هنالك نقطتان يجب اخذهما في الاعتبار عند تصنيف بيانات الاستشعار عن بعد، أولا: القصور الذي يحد من دقة خوارزميات التصنيف التقليدية عند تطبيقها على بيانات قد دمجت من متحسسات لأقمار صناعية مختلفة (بيانات الاستشعار عن بعد المتعددة المصدر (MRSD))، ثانيا: تعقيد المشهد الحضري طيفيا ومكانيا الذي يزيد من صعوبة عملية كشف التغير ومراقبته زمنياً. لذلك، يهدف هذا البحث إلى اختبار ومقارنة ثلاثة خوارزميات تصنيف (Maximum Likelihood (ML) ، Decision Trees (DT) ، و Support Vector Machines (SVM)) لقدرتها على أستنتاج واستخراج الغطاء الأرضي/الاستدلال على الأراضي في المناطق الحضرية من خلال استخدام لاندسات 5TM ، لاندسات + 7 ETM وصور ASTER ولخمس سنوات مختلفة.

أجريت مرحلة ما قبل المعالجة ومرحلة ما بعد المعالجة على كل صور مرئية فضائية بشكل منفصل والملتقطعة بخمس فترات مختلفة لنفس منطقة الدراسة للحصول على خرائط تصنيف مدينة نيوكاسل، المملكة المتحدة. بعد ذلك، تم استخدام التصنيفات الثلاثة المذكورة أعلاه وتطبيقها على البيانات المدمجة (المنصهرة)، والتي تضمنت ثلاثة وثلاثين حزمة (فرقة طيفيه) من أجل تقييم مدى فعاليتها في فصل أنواع او اصناف الغطاء الارضي في المناطق الحضرية. تم تنفيذ طريقة التصنيف باستخدام برنامج ERDAS IMAGINE والترميز بواسطة MATLAB. وتشير النتائج إلى أن دقة التصنيف الشاملة لثلاث خرائط المصنفة باستخدام المصنفات ML، DT، و SVM كانت 71.09٪، 73.05٪ و 83.20٪ على التوالي. تبين طريقة المقارنة التي اجريت لتصنيف عدد كبير من بيانات الاقمار الصناعية (MRSD) المتمثلة بدمج وانصهار ثلاثة وثلاثون حزمه طيفيه لثلاثة اقمار صناعيه مختلفة في الدقة المكانية والطيفية والزمنية على امكانية تكامل عدة مصادر من البيانات لتحسين دقة التصنيف وتعزيز امكانية فصل اصناف الغطاء الارضي بقدر أكبر من استخدام لمصدر واحد من بيانات الاستشعار عن بعد.

الكلمات الدالة: انصهار البيانات، والتعلم الآلي، تصنيف صورة، بيانات الاستشعار عن بعد متعددة المصدر، استخراج الغطاء الأرضي / استخدام الأراضي.